frontiers in Physics

TYPE Original Research
PUBLISHED 10 April 2026
DOI 10.3389/fphy.2026.1799778

OPEN ACCESS

EDITED BY
Imran Khan,
COMSATS Institute of Information Technology, Pakistan

REVIEWED BY
Ivan Cvitić,
University of Zagreb, Croatia
Kemal Gokhan Nalbant,
Beykent University, Türkiye

*CORRESPONDENCE
Darius Anriukaitis,
darius.andrikaitis@ktu.lt
Mohd Aliff Sani,
mohdaliff@unikl.edu.my
Hung Tran-Huy,
hung.tranhuy@phenikaa-uni.edu.vn

RECEIVED 30 January 2026
REVISED 24 February 2026
ACCEPTED 11 March 2026
PUBLISHED 10 April 2026

CITATION
Mohamed HG, Anriukaitis D, Konecny J, Sani MA, Tran-Huy H, Nguyen-Quang A, Qaddara I and Prauzek M (2026) A novel metasurface structure for oblique incidence absorption and ultrawideband transmission based on Haxagonal metal rings and epoxy laminate. *Front. Phys.* 14:1799778. doi: 10.3389/fphy.2026.1799778

A novel metasurface structure for oblique incidence absorption and ultrawideband transmission based on Haxagonal metal rings and epoxy laminate

Heba G. Mohamed[1], Darius Anriukaitis[2]*, Jaromir Konecny[3], Mohd Aliff Sani[4]*, Hung Tran-Huy[5]*, Anh Nguyen-Quang[5], Iyas Qaddara[6] and Michal Prauzek[3]

[1]Department of Electrical Engineering, College of Engineering, Princess Nourah Bint Abdulrahman University, Riyadh, Saudi Arabia, [2]Department of Electronics Engineering, Kaunas University of Technology, Kaunas, Lithuania, [3]Department of Cybernetics and Biomedical Engineering, VSB-Technical University of Ostrava, Ostrava, Czechia, [4]Quality Engineering Research Cluster (QEREC), Malaysian Institute of Industrial Technology, Universiti Kuala Lumpur, Johor, Malaysia, [5]Faculty of Electrical and Electronic Engineering, PHENIKAA School of Engineering, PHENIKAA University, Hanoi, Vietnam, [6]Department of Computer Science, Faculty of Information Technology, Al-Ahliya Amman University, Amman, Jordan

Introduction: Metamaterials progressed greatly due to groundbreaking studies on composite media that show both negative permeability and permittivity at the same time. This study has significantly improved our understanding of materials that can surpass the electromagnetic properties of standard substances, thereby transcending the constraints imposed by their intrinsic electromagnetic features. They have attracted considerable interest owing to their remarkable ability to manipulate EM waves through subwavelength structures organized in precise configurations. These materials are famous for their unique electromagnetic characteristics, such as negative index refraction, super-resolution imaging, and perfect absorption. The effective characteristics of metamaterials can be tailored to fulfill particular application needs—like obtaining negative permittivity and permeability—by adjusting the dimensions of a unit cell. With the EM environment becoming more complex, challenges to EM protection are increasing. Microwave absorbers made from metamaterials have come to represent a viable option for stealth technology, as they employ custom-designed structures to absorb electromagnetic waves. As two-dimensional metamaterials, metasurfaces control incident waves precisely through periodic unit designs.

Methods: This paper proposes a novel metasurface structure for absorbing oblique incident EM waves. The design composed of double layer metamaterial where the first layer consists of fiber glass which is enforced by epoxy laminate. The second layer is made up of irregular metal patches and linked by metal rings and chip resistors.

Results and Discussion: Simulation results show that the proposed metasurface has better absorption capability as compared with existing designs.

KEYWORDS
electromagnetic waves, epoxy lamination, metamaterial, metasurface, ultrawideband absorber

1 Introduction

With the rapid development of wireless communication technology and high-frequency equipment, and the increasing popularity and promotion of smart home and other electronic devices, the negative impacts of electromagnetic radiation have become increasingly complex and diverse. Utilizing electromagnetic absorption technology to eliminate electromagnetic pollution and achieve electromagnetic protection is an effective method for solving such problems. In traditional absorption technologies, resonant absorbers, represented by Salisbury screens, can only achieve electromagnetic absorption within a narrow frequency band. Although Jaumann absorbers obtained through spatial topology can broaden the absorption bandwidth, they also significantly increase the thickness of the absorber. Magnetic absorbing materials, represented by ferrites, possess certain absorption performance at relatively thin thicknesses, but cannot achieve high-performance absorption over a wide bandwidth and have a high surface density. Therefore, developing new electromagnetic absorption technologies has become a recognized important issue.

Currently, metamaterial absorbers, as a type of periodically arranged artificial composite absorbing structure, have become a research hotspot in the field of microwave absorbing technology due to their advantages such as the ability to improve absorption performance and achieve thinness through the design of structural units, which have great application prospects. Based on the properties of the structural units, metamaterial absorbers can be divided into two categories: lossless metallic unit metamaterial absorbers [1–5] and resistance-loaded unit metamaterial absorbers [6–17].

Regarding lossless metallic metamaterial absorbers: Ref. [1] proposed a metasurface absorber with an octagonal fan-shaped structural unit, which can generate a 90% absorption band with a width of 0.15 GHz on both sides of 9.26 GHz, an oblique incident angle of 70°, and a thickness of 0.8 mm. Reference [3] designed a single-layer metasurface absorber using a combined graphic structural unit, which generated five absorption peaks with extremely narrow 90% absorption bandwidths, and a thickness of 1.5 mm. Regarding resistive-loaded metamaterial absorbers: A resistive-loaded combination circular ring unit single-layer metasurface absorber with a relative bandwidth of 86.2%, an oblique incidence angle of 45°, a thickness of 3.4 mm, and a reflection coefficient of less than −10 dB in the 8.0–20.1 GHz frequency band was designed by Ref. [6]. Reference [10] added more matching layers to the design, increased the oblique incidence angle to 45°, and increased the thickness to 18.0 mm to obtain 90% absorption in the 2.3–13.3 GHz frequency region with a relative bandwidth of 141.0%. Reference [13] achieved 90% absorption with a relative bandwidth of 171.2% based on a metamaterial absorber designed with a double-layer metasurface, without considering oblique incidence stability. An absorber based on a three-layer resistively loaded metasurface that attained 90% absorption with a relative bandwidth of 170.0% and an incidence angle of 40° was proposed in Ref. [16].

Consequently, at relatively thin thicknesses, metamaterial absorbers based on lossless metallic unit metasurfaces can only produce one or more absorption peaks with an absorption rate greater than 90% and a bandwidth less than 0.5 GHz, leading to a narrow effective absorption bandwidth. However, at the expense of greater thickness, metamaterial absorbers based on resistive-loaded unit metasurfaces greatly enhance absorption performance and extend the effective absorption bandwidth. Typically, a single-layer resistive-loaded metasurface absorber can achieve a relative bandwidth of approximately 100% for its 90% absorption bandwidth, with an oblique incidence angle of approximately 30° [6–9]. The design of multilayer resistive-loaded metasurfaces [11–17] can raise the oblique incidence angle to 45° and enhance the relative bandwidth of the 90% absorption bandwidth to roughly 170%. It should be noted that although multilayer resistive-loaded metasurface absorbers achieve a broadened absorption bandwidth and an increased absorption angle, they still suffer from drawbacks such as low absorption intensity, an unsatisfactory oblique incidence angle, and exposed metasurface layers (stability risk).

This research suggests a design approach for a multilayer composite absorber based on a double-layer metasurface to overcome the aforementioned problems. The main contributions are as follows.

1. Designs a broadband wide-angle composite absorber with a protective skin layer and complementary enhancement of the double-layer metasurface.
2. The structural units of metasurfaces I and II are an irregularly shaped metal sheet connected by patch resistors and a hexagonal metal ring loaded with patch resistors, respectively.
3. Glass fiber laminate makes up the skin layer. The frequency with a reflection coefficient less than −10 dB at an oblique incidence angle of 5° is 2.36–23.87 GHz, with a relative bandwidth of 164.0%.
4. With a relative bandwidth of 152.0%, an oblique incidence angle of at least 60°, and a total thickness of 14.2 mm, the absorption frequency band of −20 dB is 3.17–23.16 GHz.
5. This design raises the incident angle, improves absorption intensity over a broad bandwidth, and lowers safety hazards because of the protective skin layer, making it appropriate for a greater variety of applications.

The remaining of this paper is organized as follows. In Section 2, the design structure and absorption procedure is discussed. In Section 3, the performance evaluation of double-layer metasurface is presented. In Section 4, the experimental results and analysis is performed. In Section 5, the conclusion is discussed.

2 Structural design and absorption mechanism

The design of the metasurface and the supporting dielectric layer make up the two primary components of metasurface absorber design. In the study of Ref. [18], our research group proposed a design method for single-layer metasurface absorbers capable of achieving a reflection coefficient below −20 dB over a wide bandwidth. This paper further studies and summarizes the design principles of a double-layer metasurface that broadens the absorption bandwidth to below −20 dB, and provides a simple discussion with design examples. First, the absorber design proposed in this study is mainly based on the quarter-wavelength resonant loss absorption mechanism and multiple interference theory [19]. Figure 1 illustrates its design logic.

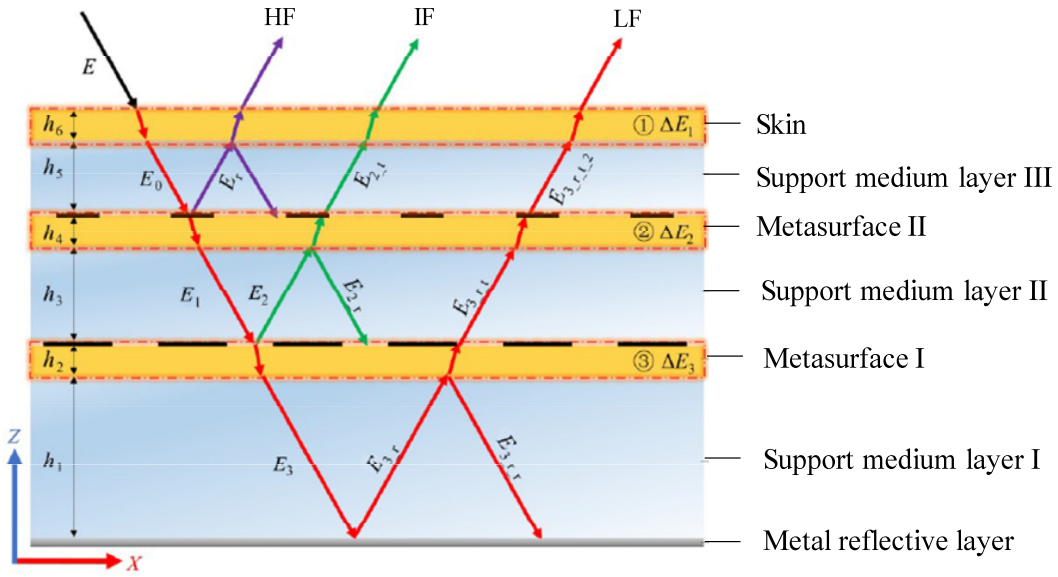

FIGURE 1
Structure and absorption mechanism of a double-layer metasurface complementary enhanced broadband wide-angle composite absorber.

When electromagnetic waves of different frequencies enter the absorber, they sequentially pass through the top skin, supporting dielectric layer III, metasurface II, supporting dielectric layer II again, metasurface I, and supporting dielectric layer I. They are reflected without loss at the metal reflective layer, and the remaining energy after passing through multiple functional layers continues to propagate. Supporting dielectric layers I, II, and III are low-loss dielectrics; metasurface I is an interface with strong electromagnetic loss and relatively strong reflection; metasurface II is an interface with strong electromagnetic loss and relatively strong reflection; and the top skin layer can be thought of as an interface with weak electromagnetic loss and weak reflection. The ultra-wideband absorber proposed in this paper, based on the quarter-wavelength resonant loss mechanism, firstly exhibits strong absorption characteristics at the locations of metasurface I and metasurface II. Secondly, utilizing the reflection characteristics of metasurfaces I and II and the loss characteristics of the skin layer, an absorption enhancement layer is added to the absorber at low, mid, and high frequencies, ultimately achieving an absorption rate greater than 99% over the ultra-wideband range.

Based on the above design principles, it can be concluded that the two metasurfaces can be regarded as two independent absorbers based on single-layer metasurfaces without considering mutual coupling. Therefore, metasurface I and metasurface II can be preliminarily designed using the design principles derived in Ref. [18], and should meet the following principles:

1. The absorption frequency bands corresponding to metasurface I and metasurface II should have a reflection coefficient of around −7.0 dB and an absorption rate of around 0.44
2. Metasurface I and Metasurface II should have complementary transmission frequency ranges and a transmission coefficient of about −3.5 dB. The transmission coefficient may be substantially lower when the absorption rate is significantly higher than 0.44. At the same time, the thickness design of the three-layer support medium can be preliminarily estimated by the following method. When all materials are equivalent to free-space, the thicknesses of $h_{1(\text{freespace})}$, $h_{2(\text{freespace})}$, $h_{3(\text{freespace})}$, $h_{4(\text{freespace})}$, $h_{5(\text{freespace})}$, and $h_{6(\text{freespace})}$ should meet the following conditions as expressed by Equations 1–3:

$$\frac{h_{1(\text{freespace})}+h_{2(\text{freespace})}+h_{3(\text{freespace})}+h_{4(\text{freespace})}+h_{5(\text{freespace})}+h_{6(\text{freespace})} \sim \lambda_{\text{L(freespace)}}}{\text{j4}} \tag{1}$$

$$\frac{h_3+h_4+h_5+h_6 \sim \lambda_{\text{M(freespace)}}}{4} \tag{2}$$

$$\frac{h_5+h_6 \sim \lambda_{\text{H(freespace)}}}{4} \tag{3}$$

The wavelength in air that corresponds to the beginning frequency of 99% absorptivity is denoted by $\lambda_{\text{L(freespace)}}$, the wavelength in air that corresponds to the center frequency of 99% absorptivity by $\lambda_{\text{M(freespace)}}$, and the wavelength in air that corresponds to the ending frequency of 99% absorptivity by $\lambda_{\text{H(freespace)}}$. The conversion formula between wavelength in air and wavelength in a medium is defined by Equations 4, 5:

$$\lambda_0 = \frac{c_0}{f} \tag{4}$$

$$\lambda_{\text{m}} = \frac{\lambda_0}{\sqrt{\varepsilon_{\text{r}}\mu_{\text{r}}}} \tag{5}$$

where f is the frequency, λ_{m} is the wavelength in the medium, ε_{r} is the relative permittivity of the medium, μ_{r} is the relative permeability of the medium, λ_0 is the wavelength in free space, and c_0 (2.99×10^8 m/s) is the speed of light.

The basic structure of the broadband wide-angle composite absorber created in this research is depicted in Figure 2 to

validate the aforementioned design process. It has a total of seven functional layers, from bottom to top: metal reflective layer, supporting medium layer I, metasurface I, supporting medium layer II, metasurface II, supporting medium layer III and top skin. They form a complete periodic structure in the plane by being closely arranged in regular hexagons. The performance parameters of the materials utilized in the double-layer metasurface complementary improved broadband wide-angle composite absorber structure are displayed in Table 1. Glass fiber laminate, which has a loss tangent of 0.025 and a relative permittivity of 4.30, is used for both the top skin and the substrate of the metasurface. All of the supporting dielectric layers are composed of PMI foam, which has a loss tangent of 0.0036 and a relative permittivity of 1.05. Continuous copper foil with a conductivity of 5.8×10^7 S/m makes up the metal reflective layer. Since the second resonant point of the hexagonal close-packed ring unit can reach three times that of the first resonant point, it can achieve a wider absorption characteristic than other ring structures [20, 21]. Therefore, the structural units of both metasurfaces of the broadband wide-angle composite absorber designed in this paper adopt a hexagonal structure. The structural unit of metasurface I in the absorber suggested in this research is depicted in Figure 2a. It is an uneven ring filled with 12 chip resistors with a resistance of R1. The structural unit of metasurface II in the absorber suggested in this research is depicted in Figure 2b. It is a regular hexagonal ring filled with six chip resistors with a resistance of R2.

The structure in this research is designed and simulated using CST Microwave Studio 2023, an electromagnetic simulation program. S-parameters are the results of the simulation. The absorptivity is determined using formula $A = 1 - |r_{yy}|^2 - |r_{xy}|^2 - |t_{xy}|^2 - |t_{yy}|^2$ where r_{yy} is the reflectivity, r_{xy} is the reflection polarization conversion rate, t_{xy} is the transmission polarization conversion rate, and t_{yy} is the transmission rate. This formula takes into account the impact of polarization conversion [22–25] on the accuracy of the structure's absorption performance characterization, as illustrated in Figure 2, if the incident electromagnetic wave has an electric field component in the y direction (corresponding to TE polarization). The absorptivity of the structure is obtained through data post-processing. In the complete ultrawideband absorbing metamaterial structure, the presence of the metallic reflective layer makes the t_{xy} transmission polarization conversion rate and t_{yy} transmission rate zero. At this point, the absorptivity formula simplifies to $A = 1 - |r_{yy}|^2 - |r_{xy}|^2$. The computation of TM wave absorptivity is comparable to that of TE wave absorptivity. The proposed design underwent multiple parameter scanning optimizations, and the final structural parameters are as follows: P = 6.1 mm, L_1 = 3.6 mm, L_2 = 1.2 mm, L_3 = 2.4 mm, L_4 = 5.2 mm, w_1 = 1.2 mm, w_2 = 1.8 mm, w_3 = 0.7 mm, w_r = 0.5 mm, h_1 = 7.0 mm, h_2 = 0.2 mm, h_3 = 4.1 mm, h_4 = 0.2 mm, h_5 = 2.4 mm, h_6 = 0.3 mm, R_1 = 80.6 Ω, R_3 = 430 Ω.

3 Performance evaluation of double-layer metasurface

The double-layer metasurface complementary enhanced broadband wide-angle composite absorber can achieve absorption performance with a reflection coefficient below −10 dB (90% absorptivity) and −20 dB (99% absorptivity) in the ultra-wideband range, according to simulation results of the suggested structure at various incident angles, as shown in Figure 3. Under TE wave conditions, the incident angle stability of −10 dB absorption is not less than 50°, and it still possesses ultra-wideband absorption characteristics at an incident angle of 60°. Under TM wave conditions, the incident angle stability of −10 dB absorption is not less than 30°, and it still possesses broadband absorption characteristics at an incident angle of 60°. Additionally, as Figures 3b,c demonstrate, the absorber's polarization conversion rate under TE/TM waves is on the order of 10^{-4}, indicating that the equivalent polarization conversion absorption has no effect on the actual absorption performance. The quarter-wavelength resonance's electromagnetic loss is the primary source of the designed absorber's excellent absorption performance. In particular, the TE/TM wave's reflection coefficient is less than −10 dB when the electromagnetic wave is incident perpendicularly. The dB has a bandwidth of 2.80–23.64 GHz. 3.56–22.56 GHz is the −20 dB absorption band. The frequency range with a reflection coefficient below −10 dB in TE wave mode at an incidence angle of 15° is 2.92–24.08 GHz, and the range with a reflection coefficient below −20 dB is 4.16–23.56 GHz. The frequency range with a reflection coefficient less than −10 dB at an incidence angle of 30° is 2.96–25.72 GHz.

The frequency bands 3.68–23.68 GHz and 26.04–29.16 GHz have reflection coefficients below −10 dB at an incidence angle of 50°, while the 7.84–21.36 GHz region has a reflection coefficient below −10 dB. The frequency ranges 6.96–23.28 GHz and 25.12–29.32 GHz have reflection coefficients less than −10 dB at an incidence angle of 60°. At an incident angle of 15° in TM wave mode, the frequency band with a reflection coefficient below −10 dB is 3.04–24.56 GHz, and the frequency band with a reflection coefficient below −20 dB is 4.48–23.72 GHz; at an incident angle of 30°, the frequency band with a reflection coefficient below −10 dB is 3.44–24.00 GHz, and the reflection coefficient is below −15 dB in the range of 4.24–21.08 GHz. At a 50° incident angle, the frequency bands with a reflection coefficient below −10 dB are 5.44–24.96 GHz and 26.40–29.12 GHz; at a 60° incident angle, the frequency range with a reflection coefficient below −10 dB is 8.12–22.96 GHz.

To demonstrate and validate the physical mechanism of the microwave absorber designed in this paper, CST Microwave Studio 2023 is used to quantitatively characterize the electromagnetic properties of metasurfaces I and II, as well as the effect of the surface skin on microwave absorption performance. First, Figure 4a depicts the electromagnetic properties of metasurface I as well as the effect of resistance on microwave absorption performance. When θ = 0°, metasurface I has an absorptivity larger than 0.44 in the range of 3.00–18.92 GHz, a reflection coefficient between −7.0 and −6.5 dB in the range of 2.92–10.16 GHz, and a transmission coefficient between −5.3 and −3.5 dB in the range of 2.08–20.20 GHz. The high reflection coefficient relates to a frequency range with much higher absorptivity than 0.44. Figure 4b depicts the reflection coefficient of a microwave absorber based on metasurface I when h_1 = 7.0 mm and various resistance values R_1 are used. The absorber has significant absorption performance in the 3.40–16.00 GHz frequency region. When R_1 = 60.0 Ω, the reflection coefficient in the middle 4.92–10.52 GHz band is greater than −10 dB. When R_1 increases to 70.0 Ω, the reflection coefficient in the middle frequency

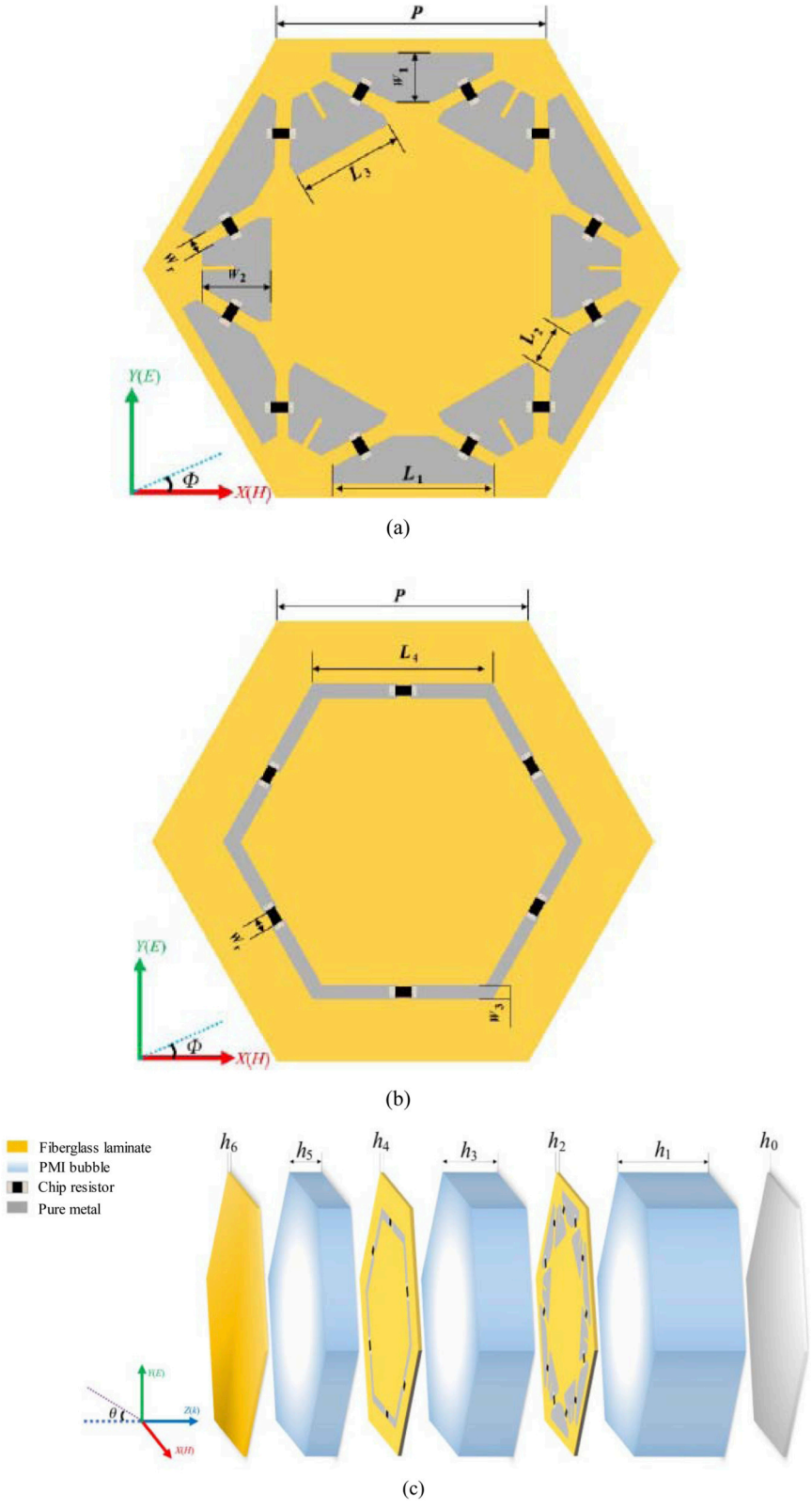

FIGURE 2
Proposed metasurface absorber structure. **(a)** Metasurface I structural unit; **(b)** metasurface II structural unit; **(c)** composite absorber structure unit.

TABLE 1 Performance parameters of materials contained in the proposed metasurface absorber.

Material	Location	Dielectric constant	Loss tangent	Electrical conductivity (S/m)
Fiberglass laminate	h_2, h_4, h_6	4.3	0.0250	—
PMI bubble	h_1, h_3, h_5	1.05	0.0036	—
Metallic copper	h_0	—	—	5.8×10^7

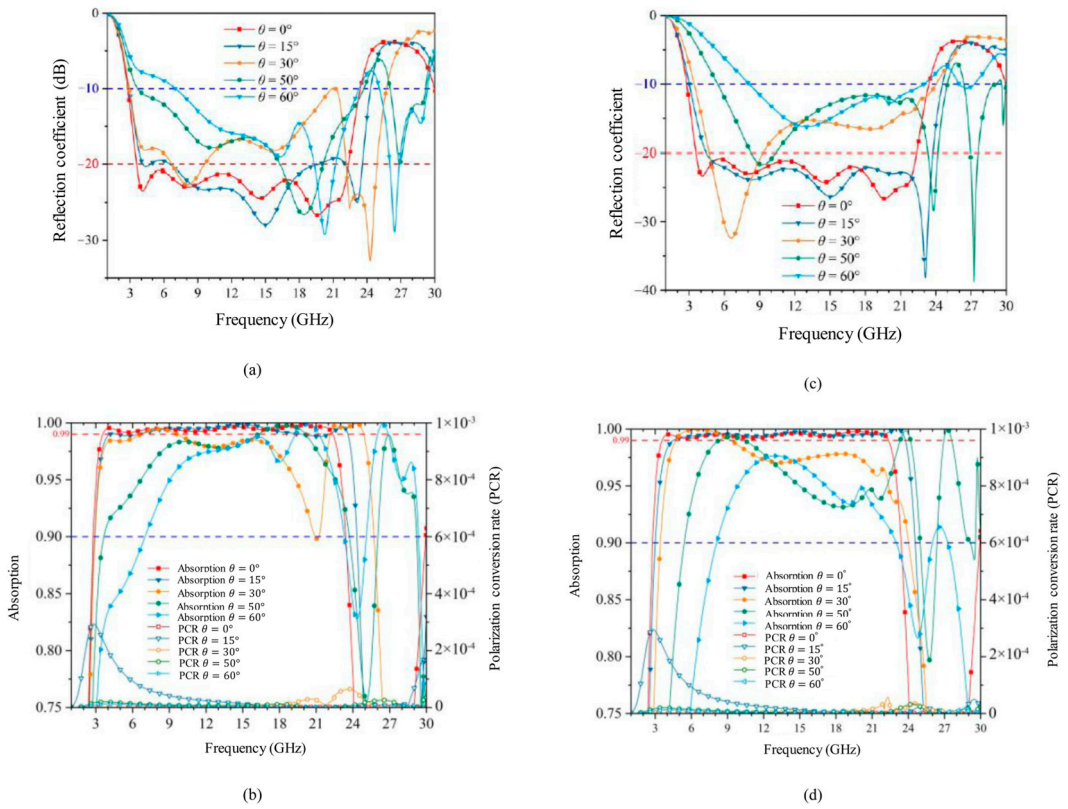

FIGURE 3
Simulation results of enhanced broadband absorber. **(a)** Reflection coefficient of TE wave at different incident angles; **(b)** absorptivity and polarization conversion rate of TE wave at different incident angles; **(c)** reflection coefficient of TM wave at different incident angles; **(d)** absorptivity and polarization conversion rate of TM wave at different incident angles.

band decreases significantly, and when R_1 = 80.0 Ω, the reflection coefficient in the 4.04–15.60 GHz band is lower than −10 dB. As R_1 further increases, the reflection coefficient in the middle frequency band of the absorber further decreases, but the effective absorption bandwidth narrows towards the middle frequency band. Meanwhile, as R_1 increases, the absorber based on metasurface I consistently exhibits significant reflection characteristics in the 17.00–26.00 GHz frequency band. Figure 4c illustrates the reflection coefficient of the absorber based on metasurface I at various incident angles, with h_1 = 7.0 m and R_1 = 80.6 Ω. As the incidence angle increases, the absorber's absorption band changes to higher frequencies, while the effective absorption band narrows. Therefore, metasurface I itself does not possess good oblique incidence stability characteristics. When the incidence angle is 15°, the frequency range with a reflection coefficient less than −10 dB is 4.44–15.80 GHz, which shifts to higher frequencies by about 0.27 GHz compared to the absorption band at 0°. When the incidence angle is increased to 30°, the frequency range with a reflection coefficient of less than −10 dB is 8.24–17.48 GHz, while the absorption band shrinks by 2.12 GHz.In addition, when the incidence angle is larger than 45°, the absorption performance of metasurface I in the high-frequency band of 19.00–29.00 GHz is improved. Therefore, metasurface I is mainly used for the absorption of electromagnetic waves in the 3.40–16.00 GHz band, and for enhanced absorption at high frequencies at large incident angles.

Next, we analyze the electromagnetic properties of metasurface II and the influence of the applied resistor on its absorption performance. Figure 5a shows that when θ = 0°, metasurface I has a higher absorptivity than 0.44 between 16.88 and 20.88 GHz, a lower reflection coefficient between 1.00 and 30.00 GHz, and a transmission coefficient between −4.7 and −3.5 dB between 15.50 and 20.60 GHz.

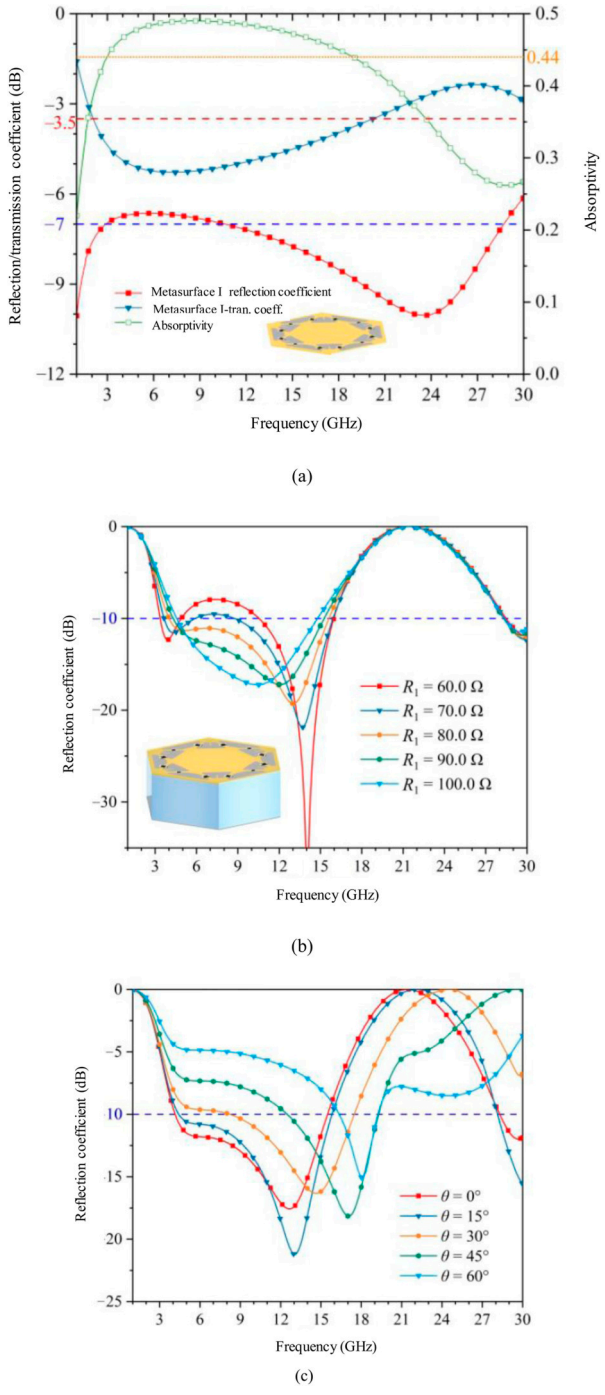

FIGURE 4
Electromagnetic properties of metasurface I. **(a)** For TE waves, with θ = 0° and R_1 = 80.6 Ω, the reflection/transmission coefficient and absorptivity of metasurface I; **(b)** TE wave, θ = 0°, reflection coefficient of absorber based on metasurface I with different resistance values R_1; **(c)** For TE waves, with R_1 = 80.6 Ω, the reflection coefficient of the absorber based on metasurface I at different incident angles.

The frequency bands with lower transmission coefficients correspond to the frequency bands with significantly higher absorptivity than 0.44. It should also be noted that metasurface II and metasurface I have complementary absorption bands and overlapping transmission bands. As shown in Figure 5b, with h_1 = 7.0 mm, h_2 = 0.2 mm, and h_3 = 4.1 mm, and without metasurface I, the reflection coefficient of the absorber based on metasurface II is shown when different resistance values R_2 are applied. As R_2 gradually increases from 350.0 Ω to 450.0 Ω. The frequency band with a reflection coefficient below −10 dB widens towards lower frequencies. As R2 gradually increases from 450.0 Ω to 550.0 Ω, the starting frequency with a reflection coefficient below −10 dB remains essentially unchanged, while the ending frequency gradually shifts towards lower frequencies. However, it should be noted that as R_2 varies over a wide range, the minimum absorption coefficient of the absorber based on metasurface II increases from −8.2 dB to −5.9 dB in the 3.00–11.00 GHz frequency range, indicating a weakening absorption performance, while maintaining significant absorption characteristics in the 15.80–22.60 GHz frequency band. Figure 5c displays the reflection coefficients of the absorber without metasurface I at various incident angles (h_1 = 7.0 mm, h_2 = 0.2 mm, h_3 = 4.1 mm, and R_2 = 430.0 Ω). As the oblique incidence angle rises, the absorber switches to higher frequencies in both the low-frequency and absorption bands. The low-frequency absorption band gets more noticeable, whereas the high-frequency absorption band fades away. Therefore, metasurface II alone does not possess good oblique incident stability characteristics. At an incident angle of 15°, the low-frequency and high-frequency absorption bands remain relatively stable. At 30°, the high-frequency reflection coefficient below −10 dB decreases to 18.48–22.36 GHz. At 60°, the high-frequency reflection coefficient below −10 dB disappears and a new low-frequency reflection coefficient band of 5.68–11.52 GHz is added. As a result, metasurface II is most commonly used.

To verify the design principle described in this paper and further validate the effectiveness of the design method, this paper uses simulation calculations to determine the increase in the absorptivity of the composite absorber when the top skin thickness h_6 = 0.3 mm under TE wave conditions. As shown in Figure 6a, when the suggested composite absorber solely incorporates metasurface I, its absorptivity is greater than 0.44 in the 3.88–17.68 GHz range with an incidence angle of less than 15°. As the oblique incidence angle increases, the frequency band with an absorptivity greater than 0.44 broadens, agreeing with the structural reflection coefficient trend seen in Figure 4c. As shown in Figure 6b, after adding the top skin, the absorptivity is greater than 0.44 in the 3.64–12.72 GHz vertical incidence range. As the oblique incidence angle increases to 60°, the frequency range with an absorptivity larger than 0.44 expands to 3.48–18.32 GHz. Figure 6c shows that under vertical incidence, the top layer skin exhibits enhanced absorption in the range of 2.36–10.04 GHz; as the oblique incidence angle increases to 60°, the frequency band with enhanced absorption widens to 2.64–15.08 GHz, achieving an absorption enhancement effect of 0–0.12 in the low and mid frequencies, consistent with the physical mechanism described in Section 2.

Figure 7 shows a comparison of the absorption enhancement effect of the top layer skin on metasurface II at different incident angles when h_6 = 0.3 mm. As illustrated in Figure 7a, the composite absorber presented in this article only incorporates metasurface II, its absorptivity ranges from 14.96 to 24 and when incident vertically is more than 0.44; as the oblique incident angle increases, the absorptivity in this frequency band gradually drops while

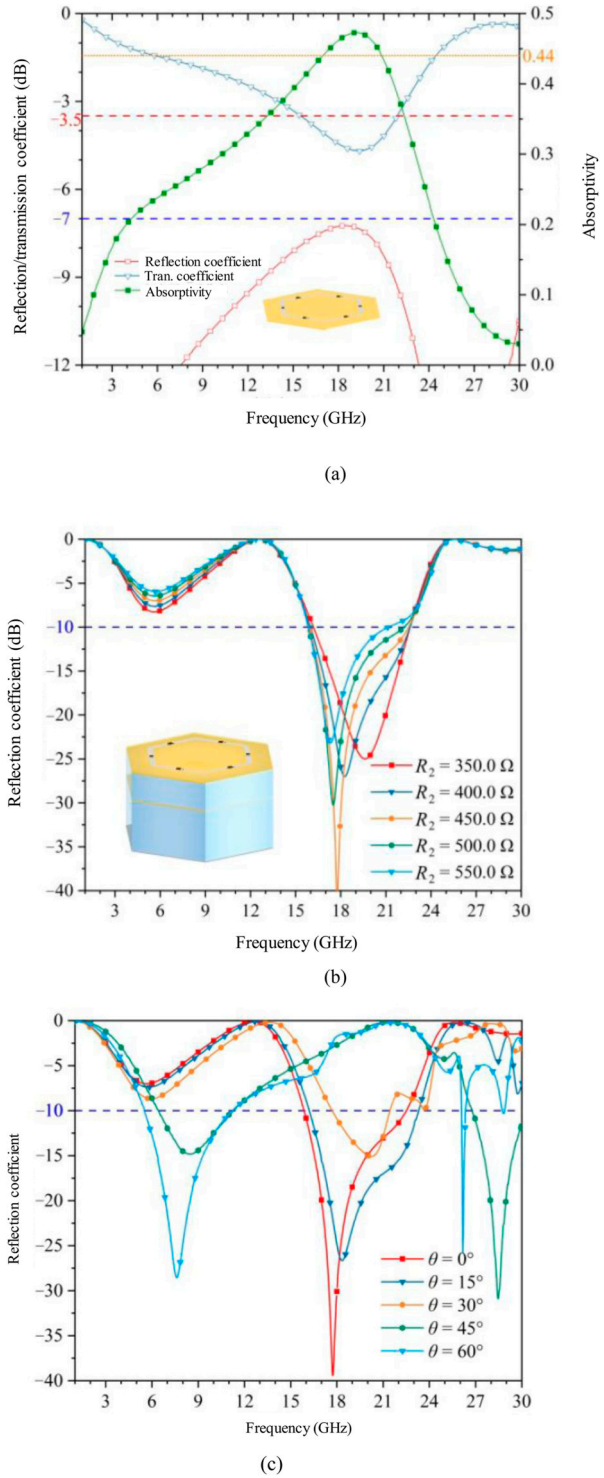

FIGURE 5
Electromagnetic properties of metasurface II. **(a)** For TE waves, θ = 0°, R_2 = 430.0 Ω, the transmission and reflection coefficient and absorptivity of metasurface II; **(b)** TE wave, θ = 0°, reflection coefficient of absorber based on metasurface II with different resistance values R_2; **(c)** For TE waves, with R_2 = 430.0 Ω, the reflection coefficient of the metasurface II at different incident angles. Therefore, metasurface II is mainly used for the absorption of electromagnetic waves in the 15.80–22.60 GHz frequency band, which complements the significant absorption band of the absorber based on metasurface I in the 3.40–16.00 GHz range. Simultaneously, metasurface II exhibits *(Continued)*

FIGURE 5 (Continued)
enhanced absorption characteristics at low frequencies with large incident angles, which complements the enhanced absorption band at high frequencies with large incident angles of the absorber based on metasurface I.

low-frequency absorptivity increases, which is consistent with the structural reflection coefficient trend in Figure 5c. As shown in Figure 7b, after adding the top layer skin, its absorptivity in the range of 14.44–23.52 GHz is greater than 0.44 when incident vertically, with a slight shift towards lower frequencies; when the oblique incident angle increases to 60°, the absorptivity in this frequency band fluctuates around 0.44. Figure 7c shows that when incident vertically, the top layer skin has a frequency range of 6.64–22.12 GHz. Absorption enhancement occurs in the GHz range; as the oblique incident angle increases to 60°, the frequency band with partially discontinuous absorption enhancement widens to 7.16\30.00 GHz, achieving an absorption enhancement effect of 0–0.22 in the mid-frequency and high-frequency ranges, consistent with the physical mechanism described in Section 2.

Figure 8 shows a comparison of the absorption enhancement effect of the top layer skin on the structures containing metasurface I and metasurface II at different incident angles when h_6 = 0.3 mm. As shown in Figure 8a, as the oblique incident angle increases, the combined structure improves oblique incident stability performance over a wide range, owing to metasurface I's low-frequency oblique incident stability and mid-to-high frequency absorption enhancement characteristics, as well as metasurface II's low-frequency absorption enhancement characteristics.

Figure 8b illustrates that adding a top layer skin while retaining oblique incidence stability boosts the composite structure's absorption rate. Figure 8c demonstrates that under vertical incidence, the top layer skin enhances absorption in the 2.52–22.56 GHz band. By increasing the oblique incidence angle to 60°, the frequency band with partially discontinuous absorption enhancement spreads to 1.00–30.00 GHz, resulting in an absorption enhancement effect of 0–0.20 in low, mid, and high frequencies.

Figure 9 compares the absorption rates of the proposed double-layer metasurface complementary improved broadband wide-angle composite absorber with and without the top layer skin, as shown in Figure 9c. Under vertical incidence, the skin layer can enhance the absorber's overall absorption rate by more than 0.01 in the 1.92–25.22 GHz range. As the oblique incidence angle increases, so does the upper limit of the frequency band with somewhat discontinuous absorption amplification, which now stands at 29.48 GHz. The maximum increase in absorption rate reached 0.42, therefore the enhanced absorption rate of the skin layer in the composite structure is consistent with the physical mechanism described in Section 2.

Furthermore, the effect of various skin thicknesses on the overall performance of the absorber is examined. As illustrated in Figure 10, when electromagnetic waves are incident perpendicularly, the reflection coefficients of the composite absorber with varying top skin thicknesses are as follows: The composite absorber presented in this study has a reflection coefficient less than −10 dB in

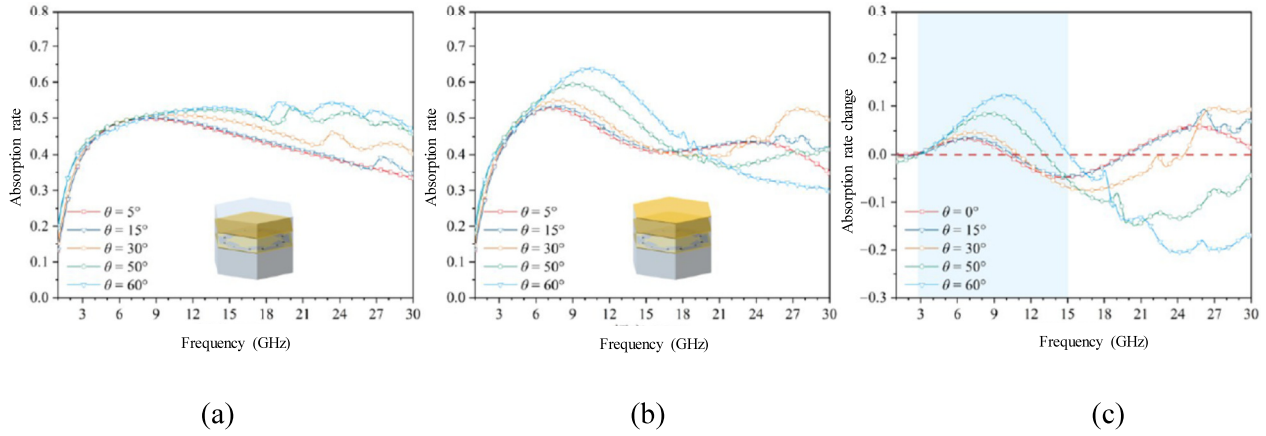

FIGURE 6
TE wave, h_6 = 0.3 mm, enhancement of absorption of metasurface I by the top layer skin at different incident angles. **(a)** Without top surface; **(b)** with top layer of surface; **(c)** changes in absorption rate with or without top layer surface.

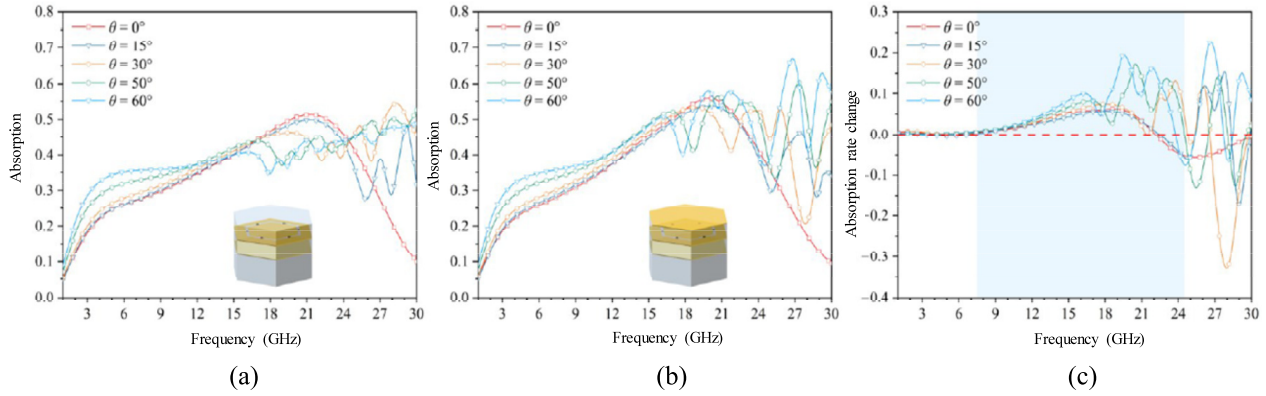

FIGURE 7
TE wave, h_6 = 0.3 mm, enhancement of absorption of metasurface II by the top layer skin at different incident angles. **(a)** Without top layer; **(b)** with top layer; **(c)** change in absorption rate with and without top skin.

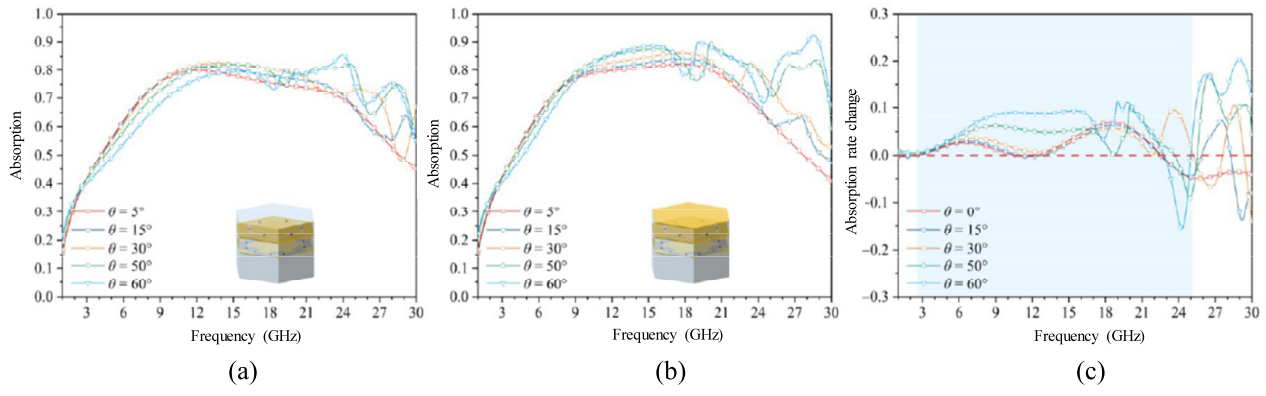

FIGURE 8
For TE waves, h_6 = 0.3 mm, at different incident angles, the top layer skin provides overall absorption enhancement for both metasurface I and metasurface II. **(a)** Without top layer; **(b)** with top layer; **(c)** change in absorption rate with and without top skin.

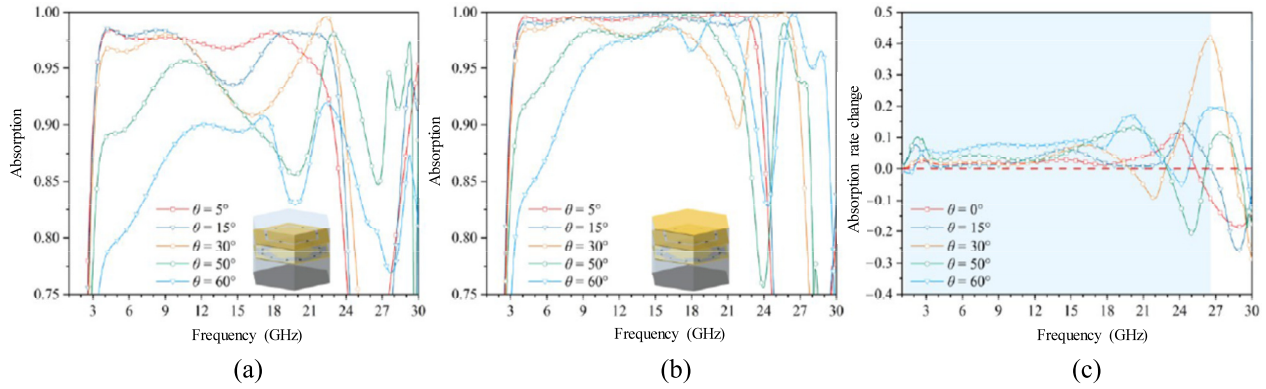

FIGURE 9
TE wave, h_6 = 0.3 mm, the absorption enhancement effect of the top layer skin on the proposed absorber at different incident angles. **(a)** Without top layer; **(b)** with top layer; **(c)** change in absorption rate with and without top skin.

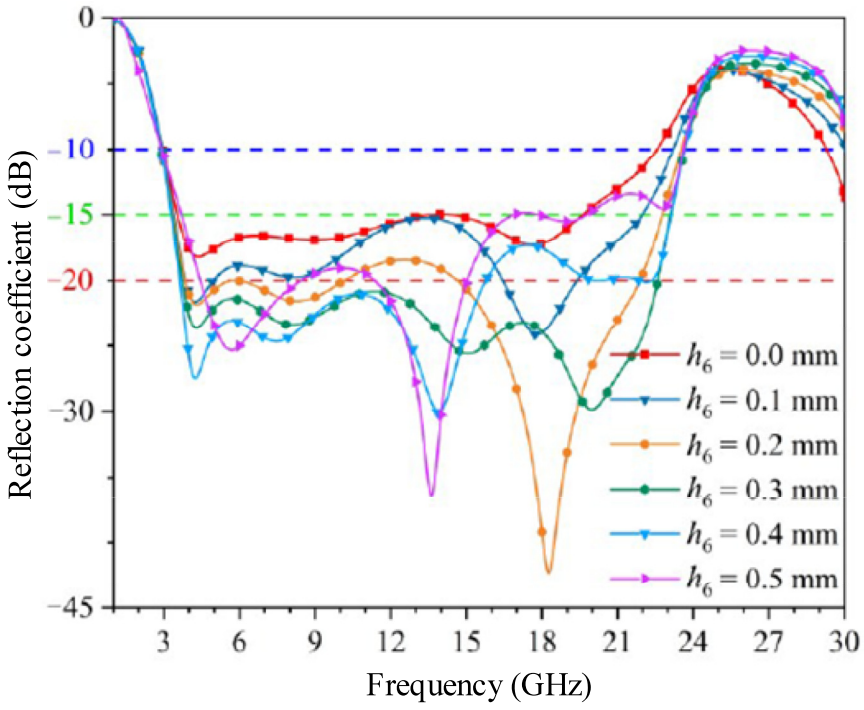

FIGURE 10
TE wave, reflection coefficient of the absorber at different skin thicknesses h_6 when θ = 0°.

the frequency band of 2.80–23.64 GHz and less than −15 dB in the frequency band of 3.20–22.84 GHz without a top skin [28, 29]. As skin thickness increases from 0.1 mm to 0.6 mm, the frequency range with a reflection coefficient less than −10 dB spreads to the largest point, 2.89–23.67 GHz, with few modifications. Furthermore, when the skin thickness ranges between 0.3 and 0.6 mm, the frequency band with a reflection coefficient of less than −10 dB remains nearly constant. As skin thickness increases from 0.1 mm to 0.4 mm, the frequency band with a reflection coefficient of less than −15 dB steadily widens, peaking at 0.4 mm. The broadest reflectance band below −20 dB (3.73–22.59 GHz) is created at a thickness of 0.3 mm, and the wavelength range is 3.29–23.14 GHz. The bands with reflectance below −15 dB and below −20 dB steadily narrow as the skin thickness grows from 0.4 mm to 0.6 mm [30]. Therefore, the significance of the top layer skin lies in its ability to significantly enhance the absorption intensity of the composite absorber and improve its stability under oblique incidence. In addition, the addition of the top layer skin avoids and reduces the potential risks of exposed metasurface II in the environment, such as structural damage from impacts and device drop, thus improving the environmental adaptability of the metamaterial absorber.

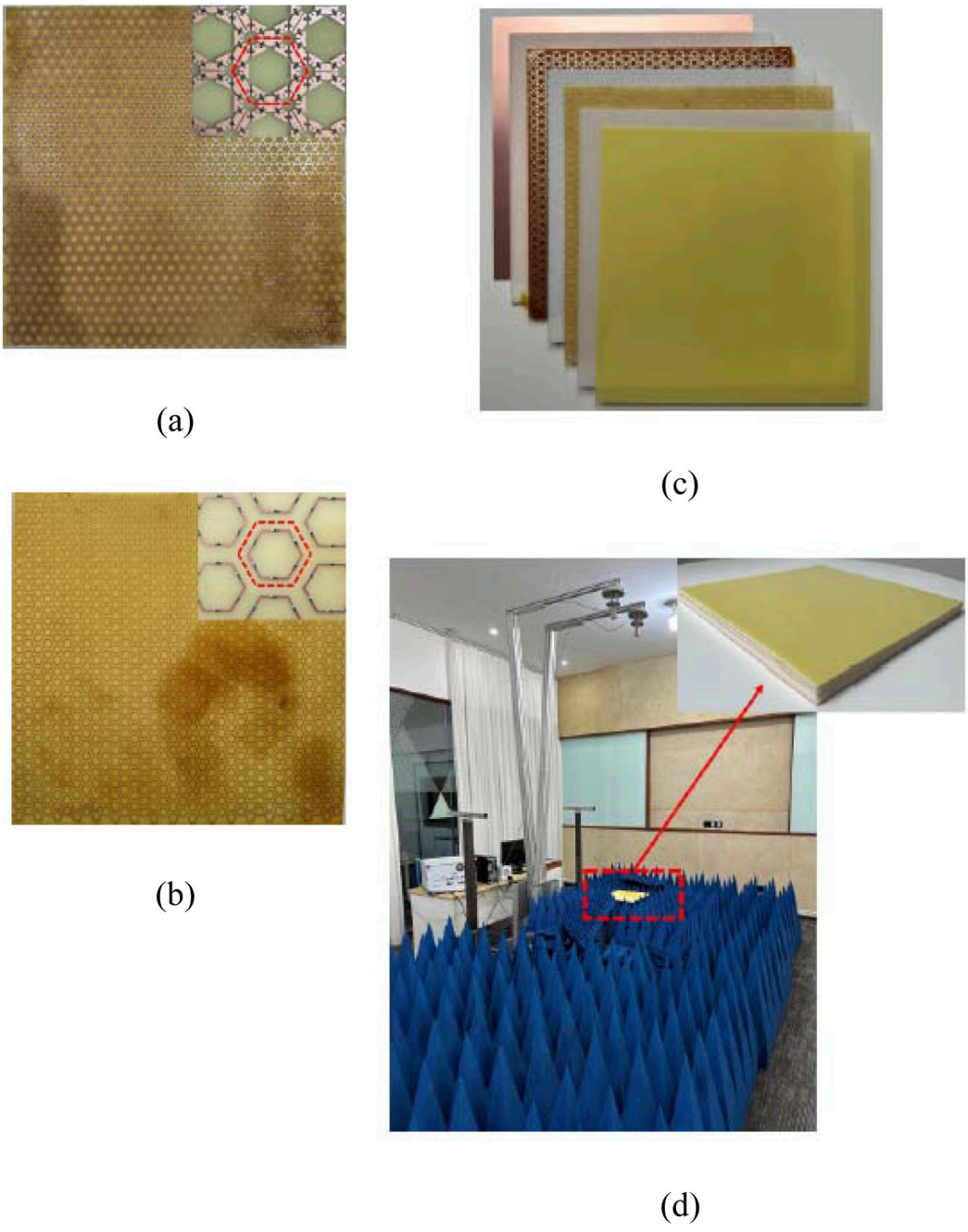

FIGURE 11
Physical specimen and testing environment of broadband wide-angle composite absorber. **(a)** Metasurface I physical image; **(b)** Metasurface II physical image; **(c)** Physical images of various parts of a broadband wide-angle composite absorber **(d)** experimental measurement setup.

4 Experimental results and analysis

To verify the proposed dual-layer metasurface complementary enhanced broadband wide-angle composite absorber, our research group fabricated a 305 mm × 305 mm flat plate sample containing 986 basic units. The physical samples of metasurface I, metasurface II, and other components of the broadband wide-angle composite absorber are shown in Figures 11a–c. A semi-open microwave anechoic chamber was used to measure the sample. The reflection coefficient of the sample was tested at various incident angles using a bow-shaped method testing equipment and a Ceyear 3671G vector network analyzer. The sample's testing environment is depicted in Figure 11d.

Figures 12a,c show the reflection coefficients of the sample at different incident angles. Under TE wave conditions, at incident angles of 5° and 15°, the −20 dB absorption bands are 3.17–23.16 GHz and 3.55–23.68 GHz, respectively. At incident angles of 5°, 15°, 30°, 50°, and 60°, the −10 dB

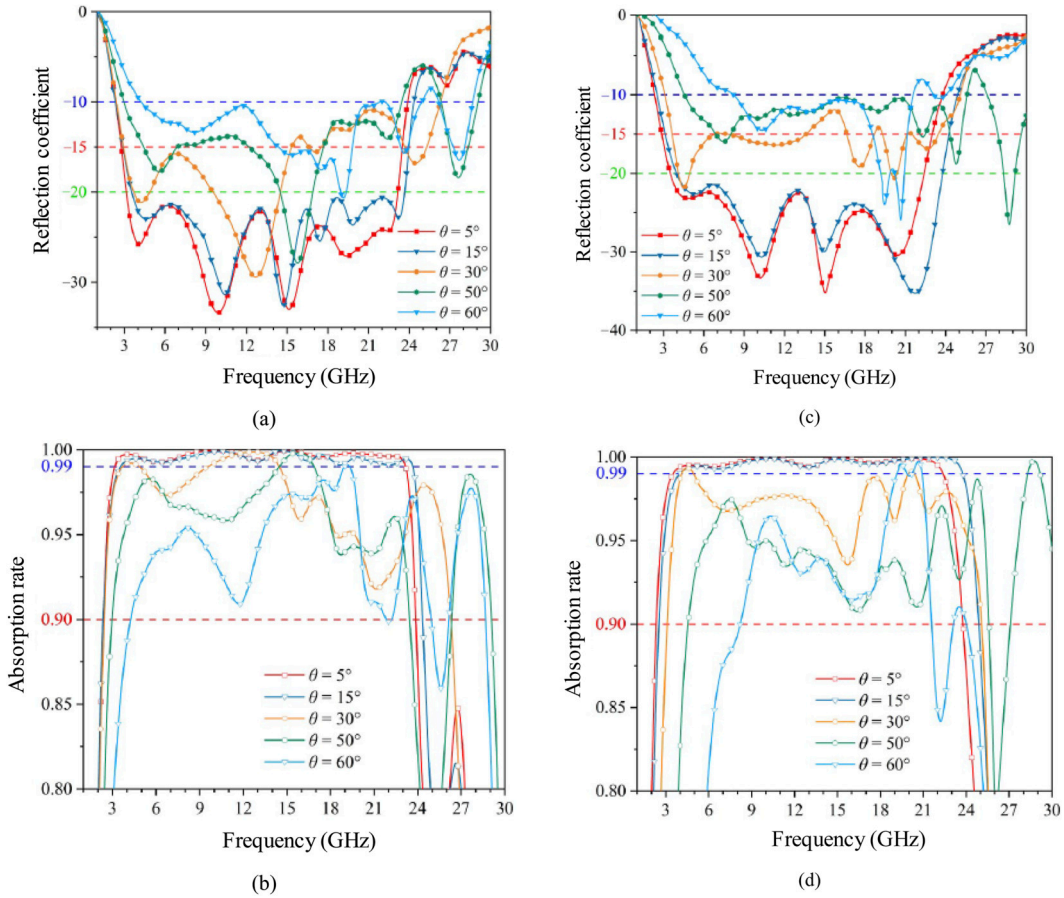

FIGURE 12
Results of absorber measurements and calculations at various incidence angles. **(a)** Reflection coefficient measurement at different incident angles under TE waves; **(b)** absorption rate measurement at different incident angles under TE waves; **(c)** reflection coefficient measurement at different incident angles under TM waves; **(d)** absorption rate measurement at different incident angles under TM waves.

TABLE 2 **Comparison of broadband absorber performance.**

Ref.	Vertical incidence relative bandwidth (GHz)		Maximum angle of incidence				Absolute thickness (mm)	Relative thickness λL (mm)
	−10 dB	−20 dB	−10 dB		−20 dB			
			TE	TM	TE	TM		
[10]	$[f_L = 2.3, f_H = 13.3]$ 141%	—	45°	45°	—	—	18	0.138
[13]	$[f_L = 1, f_H = 12.9]$ 171.2%	—	0°	0°	—	—	26	0.087
[16]	$[f_L = 5.2, f_H = 44]$ 158%	—	0°	0°	—	—	6.5	0.120
[18]	$[f_L = 6.1, f_H = 18]$ 117%	$[f_L = 7, f_H = 18]$ 88%	50°	40°	40°	30°	8	0.155
[26]	$[f_L = 11.9, f_H = 45.3]$ 117%	—	45°	30°	—	—	6.1	0.086
[27]	$[f_L = 2.1, f_H = 37.5]$ 178.8%	—	0°	0°	—	—	14	0.098
Proposed	$[f_L = 2.4, f_H = 23.9]$ 164%	$[f_L = 3.2, f_H = 23.2]$ 152%	60°	50°	15°	15°	14.2	0.114

absorption bands are 2.36–23.87 GHz, 2.47–24.33 GHz, 2.52–26.29 GHz, 2.97–23.45 GHz/26.35–29.08 GHz, and 4.24–24.92 GHz/26.17–28.68 GHz, respectively. Under TM wave conditions, at incident angles of 5° and 15°, the −20 dB. The absorption bands are 3.51–22.39 GHz and 3.97–23.76 GHz, respectively.

At incident angles of 5°, 15°, 30°, 50°, and 60°, the −10 dB absorption bands are 2.34–21.28 GHz, 2.52–24.88 GHz,

3.10–25.08 GHz, 4.56–25.59 GHz/27.09–30.00 GHz, and 8.21–21.58 GHz, respectively. With absorption performance with reflection coefficients below −10 dB and −20 dB in the ultra-wideband region, as well as steady features at large angles of oblique incidence, the test findings agree with the simulation results. However, the absorption onset frequency shifts slightly to lower frequencies. The possible reasons are as follows: Initially, during the simulation phase, a glass fiber laminate with a relative permittivity of 4.30 and a loss tangent of 0.025 was employed for the top skin and metasurface substrate, while a material with a relative permittivity of 1.05 and a loss tangent of 0.0036 was chosen for the supporting dielectric layer. However, in the actual sample preparation process, there may be some differences between the dielectric property test samples and the reflection coefficient test samples. Second, the supporting dielectrics of different thicknesses were obtained through a cutting machine, which introduces certain process errors. Furthermore, the thickness error increases during sample stacking and composite processes, further affecting the test results. Third, the metasurface was obtained through outsourced processing, and the fabrication process cannot guarantee that its substrate thickness and dielectric properties are completely consistent with the design values, which also affects the results. In conclusion, the effectiveness of the suggested double-layer metasurface complementary enhanced broadband wide-angle composite absorber and the viability of this design approach are clearly demonstrated by the consistency between the simulation and test findings.

To illustrate the superiority of this design, this paper compares representative ultra-wideband metamaterial absorbers from the literature of the past 2 years, mainly in terms of absorption bandwidth with reflection coefficients below −10 dB/−20 dB, maximum oblique incidence angle, and thickness, as shown in Table 2. The following conclusions are obtained: (1) The main research direction of existing absorbers is to achieve absorption with reflection coefficients below −10 dB in the ultra-wideband range, with only a very few broadband designs with reflection coefficients below −20 dB; (2) In order to broaden the −10 dB absorption bandwidth as much as possible, some designs usually sacrifice oblique incidence stability, and the maximum oblique incidence angle of some designs can reach 45°; (3) Due to the quarter-wavelength resonant absorption mechanism, the relative thickness of the absorber usually fluctuates around $0.1\lambda_L$ (the wavelength associated with a frequency having a reflection coefficient less than −10 dB is denoted by λ_L). Increasing the thickness usually brings better oblique incidence stability or a higher −10 dB absorption bandwidth. The design proposed in this paper not only achieves absorption performance of −10 dB (FBW = 164.0%) and −20 dB (FBW = 152.0%) in the ultra-wideband range, but also achieves a maximum oblique incidence angle of 60°/50° under TE/TM waves, without significantly increasing the overall thickness of the structure, demonstrating excellent comprehensive performance.

5 Conclusion

In this paper, a design technique for a multilayer composite absorber based on a double-layer metasurface is proposed, and a multilayer composite absorber with a skin protection layer and a double-layer metasurface is designed. This design method shows that the design of metasurface I and metasurface II should meet their absorption frequency band requirements, with a reflection coefficient of approximately −7.0 dB and an absorptivity of approximately 0.44. Furthermore, the transmission frequency bands of metasurface I and metasurface II should be complementary, and the transmission coefficient should be approximately −3.5 dB. Simultaneously, based on the quarter-wavelength resonant loss mechanism, adding a skin of appropriate thickness to the absorber, and adding an absorption enhancement layer at low, mid, and high frequencies, can improve the absorption performance over an ultra-wideband range. Additionally, the absorber's oblique incidence stability is improved by the top skin's absorption improvement at various incident angles. According to simulation data, the skin layer can raise the absorber's overall absorptivity by more than 0.01 in the 1.92–29.48 GHz range, with a maximum increase of 0.42 at certain frequency points. The absorber described in this study may achieve a reflection coefficient below −10 dB in the frequency range of 2.36–23.87 GHz with a relative bandwidth of 164.0% under vertical incidence, according to experimental results. With an oblique incidence angle of at least 60° and a relative bandwidth of 152.0%, the −20 dB absorption band is located between 3.17 and 23.16 GHz. Metasurface I is mostly used to improve high-frequency absorption at large incidence angles and to absorb electromagnetic waves in the 3.4–16.0 GHz region. Metasurface II is mainly used for the absorption of electromagnetic waves in the 15.8–22.6 GHz band and for enhancing low-frequency absorption at large incidence angles. Therefore, the design method and absorber proposed in this paper solve the problems of strong absorption and stability at large incidence angles in the ultra-wideband range, and also exhibit good environmental stability, providing a useful approach for the design of electromagnetic absorbers.

Data availability statement

The original contributions presented in the study are included in the article/supplementary material, further inquiries can be directed to the corresponding authors.

Author contributions

HM: Validation, Formal Analysis, Data curation, Methodology, Visualization, Writing – review and editing, Conceptualization, Investigation, Writing – original draft, Resources, Software. DA: Investigation, Writing – review and editing, Project administration, Supervision, Validation, Writing – original draft, Data curation, Visualization, Conceptualization, Resources, Formal Analysis. JK: Methodology, Writing – original draft, Investigation, Visualization, Formal Analysis, Conceptualization, Supervision, Resources, Writing – review and editing, Project administration. MS: Software, Methodology, Project administration, Writing – original draft, Formal Analysis, Resources, Data curation, Visualization, Investigation, Conceptualization, Writing – review and editing, Validation, Funding acquisition, Supervision. HT-H: Validation, Writing – review and editing, Resources, Formal Analysis,

Supervision, Methodology, Conceptualization, Software, Data curation, Writing – original draft, Visualization. AN-Q: Funding acquisition, Writing – review and editing, Writing – original draft, Supervision, Investigation, Project administration, Resources, Conceptualization, Validation, Methodology. IQ: Methodology, Validation, Project administration, Writing – review and editing, Conceptualization, Writing – original draft, Investigation, Resources. MP: Methodology, Conceptualization, Writing – original draft, Validation, Visualization, Resources, Project administration, Writing – review and editing, Software.

Funding

The author(s) declared that financial support was received for this work and/or its publication. Princess Nourah bint Abdulrahman University Researchers Supporting Project number (PNURSP2026R140), Princess Nourah bint Abdulrahman University, Riyadh, Saudi Arabia. The authors would like to express their deepest gratitude to Universiti Kuala Lumpur (UniKL) for the invaluable support toward the completion and publication of this paper. This article has been produced with the financial support of the European Union under the REFRESH–Research Excellence For REgion Sustainability and High-tech Industries project number CZ.10.03.01/00/22_ 003/0000048 via the Operational Programme Just Transition.

Conflict of interest

The author(s) declared that this work was conducted in the absence of any commercial or financial relationships that could be construed as a potential conflict of interest.

Generative AI statement

The author(s) declared that generative AI was not used in the creation of this manuscript.

Any alternative text (alt text) provided alongside figures in this article has been generated by Frontiers with the support of artificial intelligence and reasonable efforts have been made to ensure accuracy, including review by the authors wherever possible. If you identify any issues, please contact us.

Publisher's note

References

1. Deng G, Lv K, Sun H, Yin Z, Yang J. Stereo perfect metamaterial absorber based on standing gear-shaped resonant structure with wide-incident-angle stability. *Front Phys* (2020) 8:1–7. doi:10.3389/fphy.2020.609527

2. Mahmud S, Islam S, Mat K, Chowdhury M, Rmili H, Islam M. Design and parametric analysis of a wide-angle polarization-insensitive metamaterial absorber with a star shape resonator for optical wavelength applications. *Results Phys* (2020) 18:1–13. doi:10.1016/j.rinp.2020.103259

3. Islam M, Islam T, Moniruzzaman M, Samsuzzaman M, Arshad H. Penta band single negative meta-atom absorber designed on square enclosed star-shaped modified split ring resonator for S-C-X- and Ku-bands microwave applications. *Scientific Rep* (2021) 11(1–13):8784. doi:10.1038/s41598-021-87958-6

4. Amiri M, Tofigh F, Shariati N, Lipman J, Abolhasan M. Wide-angle metamaterial absorber with highly insensitive absorption for TE and TM modes. *Scientific Rep* (2020) 13(1):1–15. doi:10.1038/s41598-020-70519-8

5. Hannan S, Islam T, Almutairi A, Faruque MRI. Wide bandwidth angle- and polarization-insensitive symmetric metamaterial absorber for X and Ku band applications. *Scientific Rep* (2020) 10:1–16. doi:10.1038/s41598-020-67262-5

6. Singh A, Gupta N. Screen-printed wideband absorber for the X and Ku bands. *IEEE Trans Electromagn Compatibility* (2022) 64(5):1321–9. doi:10.1109/temc.2022.3180745

7. Sambhav S, Ghosh J, Singh A. Ultra-wideband polarization insensitive thin absorber based on resistive concentric circular rings. *IEEE Trans Electromagn Compatibility* (2021) 63(5):1333–40. doi:10.1109/temc.2021.3058583

8. Zhao Y, Chen B, Wu B. Miniaturized periodicity broadband absorber with a via-based hybrid metal-graphene structure for large-angle RCS reduction. *IEEE Trans Antennas Propagation* (2022) 70(4):2832–40. doi:10.1109/tap.2021.3125384

9. Yuan X, Zhang C, Chen M, Cheng Q, Cheng X, Huang Y, et al. Wideband high-absorption electromagnetic absorber with chaos patterned surface. *IEEE Antennas Wireless Propagation Lett* (2019) 18(1):197–201. doi:10.1109/lawp.2018.2886049

10. He F, Si K, Li R, Zha D, Dong J, Miao L, et al. Broadband frequency selective surface absorber with dual-section step-impedance matching for oblique incidence applications. *IEEE Trans Antennas Propagation* (2021) 69(11):7647–57. doi:10.1109/tap.2021.3070065

11. Chen J, Shang Y, Liao C. Double-layer circuit analog absorbers based on resistor-loaded square-loop arrays. *IEEE Antennas Wireless Propagation Lett* (2018) 17(4):591–5. doi:10.1109/lawp.2018.2805333

12. Wei J, He Y, Bie S, Wu S, Lei Z, Deng W, et al. Flexible design and realization of wideband microwave absorber with double-layered resistor loaded FSS. *J Phys D: Appl Phys* (2019) 52(18):1–14. doi:10.1088/1361-6463/ab053a

13. Yao Z, Xiao S, Li Y, Wang B. On the design of wideband absorber based on multilayer and multiresonant FSS array. *IEEE Antennas Wireless Propagation Lett* (2021) 20(3):284–8. doi:10.1109/LAWP.2020.3046010

14. Tayde Y, Saikia M, Srivastava K, Ramakrishna SA. Polarization-insensitive broadband multilayered absorber using screen printed patterns of resistive ink. *IEEE Antennas Wireless Propagation Lett* (2018) 17(12):2489–93. doi:10.1109/lawp.2018.2879274

15. Lim D, Lim S. Ultrawideband electromagnetic absorber using sandwitched broadband metasurfaces. *IEEE Antennas Wireless Propagation Lett* (2019) 18(9):1887–91. doi:10.1109/lawp.2019.2932399

16. Liu T, Kim S. Ultrawide bandwidth electromagnetic wave absorbers using a high-capacitive folded spiral frequency selective surface in a multilayer structure. *Scientific Rep* (2019) 9:164–73. doi:10.1038/s41598-019-52967-z

17. Wei Y, Chen Y, Li Y, Li F, Wu Q, Wang J, et al. Ultra-broadband 3D metamaterial microwave absorber based on split-ring structure loaded with resistors and magnetic material. *J Electron Mater* (2023) 52:6699–707. doi:10.1007/s11664-023-10598-1

18. Ma Z, Jiang C, Cao W, Li J, Huang X. An ultrawideband and high-resolution circuit-analog absorber with incident angle-insensitive performance. *IEEE Trans Antennas Propagation* (2022) 70(1):9376–84. doi:10.1109/tap.2022.3177490

19. Sepehripour F, Karimi P, Khavasi A. Wideband and polarization-independent antireflection coating using metamaterials. *IET Optoelectronics* (2020) 14(5):1–14. doi:10.1049/iet-opt.2019.0116

20. Han Y, Liao S, Xiu X, Li B, Chang Y, Xue Q, et al. Bandstop frequency selective surfaces based on aramid paper honeycomb structure. *IEEE Trans Antennas Propagation* (2022) 70(9):8164–72. doi:10.1109/tap.2022.3164209

21. Agrawal A, Kumar A, Panwar R. Resistive ink derived FSS-based microwave absorber using equivalent circuit modelling-interfaced deep learning. *Appl Phys A* (2025) 131(103):1–15. doi:10.1007/s00339-024-08216-w

22. Shi Y, Chu P, Meng Z. Ultra-wideband hybrid polarization conversion-absorption metasurface with a transmission window and narrow transition bands. *J Phys D: Appl Phys* (2023) 56(9):1–13. doi:10.1088/1361-6463/acbaa9

23. Guo Z, Gao C, Zhang H. Direction-dependent Janus metasurface supported by waveguide structure with spoof surface plasmon polariton modes. *Adv Mater Tech* (2023) 8(2):1–13. doi:10.1002/admt.202200435

24. Liao S, Qiao Z, Sui J, Zhang H. Multifunctional device for circular to linear polarization conversion and absorption. *Annalen Der Physik* (2023) 535(7):1–11. doi:10.1002/andp.202300195

25. Liao S, Sui J, Zhang H. Switchable ultra-bradband absorption and polarization conversion metasurface structure controlled by light. *Opt Express* (2022) 30(19):34172–87. doi:10.1364/OE.472336

26. Tirkey M, Gupta N. A novel ultrathin checker-board inspired ultrawideband metasurface absorber. *IEEE Trans Electromagn Compatibility* (2022) 64(1):66–74. doi:10.1109/temc.2021.3091767

27. Li Y, Gu P, He Z, Cao Z, Cao J, Leung KW, et al. An ultra-wideband multilayer absorber using an equivalent circuit-based approach. *IEEE Trans Antennas Propagation* (2022) 70(1):11911–21. doi:10.1109/tap.2022.3213415

28. Ngobeh J, Sorathiya V, Alharbi A. MXene resonator-based highly efficient ultrawideband absorber for thermal and solar absorber application. *Appl Phys B* (2025) 131(189):1–14. doi:10.1007/s00340-025-08553-5

29. Shahnawaz M, Baskey H, Akhtar J. Ultrawideband hybrid metasurface absorber using VO_2 and graphene-based FSS for THz applications. *J Appl Phys* (2025) 137:1–10. doi:10.1063/5.0269680

30. Maurya N, Ghosh J, Subramanian S, Pareek P, Singh L, Srinivas K. Tunable ultra-wideband graphene metasurface absorber: a mode merger design approach for terahertz applications. *Opt Commun* (2024) 550:1–10. doi:10.1016/j.optcom.2023.129991